VIII International Conference on Fracture Mechanics of Concrete and Concrete Structures
FraMCoS-8
J.G.M. Van Mier, G. Ruiz, C. Andrade, R.C. Yu and X.X. Zhang (Eds)

STUDY OF EVOLUTION OF FRACTURE PROCESS ZONE IN CONCRETE BY SIMULTANEOUS APPLICATION OF DIGITAL IMAGE CORRELATION AND ACOUSTIC EMISSION

SYED YASIR ALAM[*†], JACQUELINE SALIBA[†] AND AHMED LOUKILI[†]

[*] National University of Computer and Emerging Sciences
Department of Civil Engineering, Lahore, Pakistan.
E-mail: yasir.alam@nu.edu.pk, web page: http://www.nu.edu.pk

[†] L'UNAM Université, Institut de Recherche en Génie Civil et Mécanique (GeM), UMR-CNRS 6183,
Ecole Centrale de Nantes, France
Email: ahmed.loukili@ec-nantes.fr - Web page: http://www.ec-nantes.fr

Key words: Crack Opening, Fracture Process Zone, Digital Image Correlation, Acoustic Emission, Size Effect.

Abstract: In order to build sustainable structures, the study of mechanical behavior must integrate with local phenomena, e.g. fracture and strain localization. The fracture usually develops in the form of main crack, with branches, secondary cracks and the microcracking zone ahead. Various experimental methods are already employed to detect the fracture process. In this study, digital image correlation is used to measure displacement field in the cracking area. Using displacement field data, crack opening at various locations of crack is measured. The location of crack tip is estimated using crack opening data. Acoustic Emission technique is applied simultaneously with digital image correlation to identify the size of microcracking zone ahead of the propagating crack. It is observed that the two techniques in coupled position proved effective in identifying the fracture process zone and cracking mechanisms of concrete.

1 INTRODUCTION

Cracking in concrete is a major problem in the design of concrete structures. Linear fracture laws and strength based theories are limited in application to concrete because of the sizeable fracture process zone and the inelastic growth of crack openings and crack length.

Various experimental methods are already employed to detect the fracture process as the holographic interferometry, the dye penetration, the scanning electron microscopy, the acoustic emission etc. Such methods offer either the images of the material surface to observe micro-features of the concrete with qualitative analysis, or the black-white fringe patterns of the deformation on the specimen surface, from which it is difficult to observe profiles of the damaged material.

Complete fracture behaviour can be described by two parts of cracking zone. First part is the main crack or macro-crack of significant crack length and crack openings. Second part is the microcracking zone of non-negligible size but presenting negligible crack openings. However, there is another intermediate zone between main crack and microcracking zone where distributed cracks are present and crack openings are also significant. In this study growth of above cracking zones is investigated using two experimental techniques: Digital Image Correlation (DIC) and Acoustic Emission (AE). Different features of the cracking zones

are studied at important loading stages. It is observed that the two techniques in coupled position proved effective in identifying the fracture process zone and cracking mechanism of concrete.

2 EXPEIMENTAL METHOD

2.1 Materials and Specimens

ASTM type I cement with 28 days strength of 52.5 MPa was used. Coarse aggregates were crushed limestone with maximum size of 12 mm. The mix proportion is shown in the table 1. The cylinder strength of concrete at 28 days was 45 MPa.

Table 1: Proportions of concrete constituents in kg/m^3

Constituents	Dosage (kg/m^3)
Cement	312
Sand	820
Coarse aggregate	1100
Water	190

The specimens were beams with a thickness of 100 mm, depth of 200 mm and length of 800 mm. The beams were notched at mid-span with a notch-to-depth ratio of 0.2. The notch was created using a rigid non-stick Teflon strip of 3 mm thickness.

2.2 Loading system and experimental setup

The beams were tested in three point bending as shown in figure 1. Load was applied with a central jack of a closed loop universal testing machine of 160 kN capacity. The tests were electronically operated with a controlled notch mouth opening rate of 0.05 µm/s. The notch mouth opening was measured using a Crack Mouth Opening Displacement (CMOD) gauge.

In our experimental program, the digital images were acquired continuously as the specimens were loaded. Two digital cameras with 75 mm macro lens were mounted to capture images of both faces of the beam. The digital cameras have a resolution of 1040 x 1392 pixels and give 256 levels of gray output. Two series of tests were performed. In the first series, the cameras are mounted in order to image an area of approx. 60 x 100 mm² above the notch of beam. At this location, notch opening and initial crack profile were captured. For this resolution, one pixel in the image represents approx. 35 µm square on the specimen, which is considered sufficient to determine a displacement measurement with 2 µm accuracy [1].

Figure 1: Experimental setup

In the second series, the cameras were mounted at a distance required to observe the full height of the specimen with a resolution of 1 pixel = 180 µm. The images were taken at a rate of 6 images per minute for each camera. The images were stored in the system and were analyzed afterwards. The resolution of the system depends directly on the distribution of gray levels which depends on the texture of the material. A speckle pattern of black and white paint was sprayed onto the surface of specimen to improve the displacement resolution.

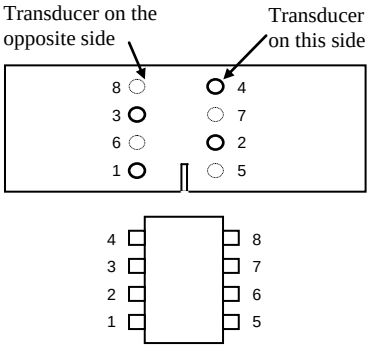

Figure 2: Position of piezoelectric sensors on the faces of specimen.

In this study, a 3D analysis of AE during tests is performed. The device for the acquisition and signal processing of AE consists of a data acquisition system MISTRAS 8 channels. For this, it is necessary to use 6-8 piezoelectric sensors (depending on the size of the sample tested) with a frequency of 50-200 kHz and a resonance frequency of 150 kHz. The sensors are placed on the beam around the area of crack propagation. Thus, the sensors form a parallelogram grid location (12 x 10 cm^2) on one side (figure 2). The signals were amplified by an amplifier with a gain of 40 dB. A detection limit of 35 dB was chosen to filter background noise. For the source to be located in 3D, a wave must reach at least four sensors. An algorithm AEWin is used for locating acoustic events. The details of the algorithm are explained in [2,3]. Location accuracy is measured in the range of 5 mm (figure 3) using the source HSU-Nielsen (NF EN 1330).

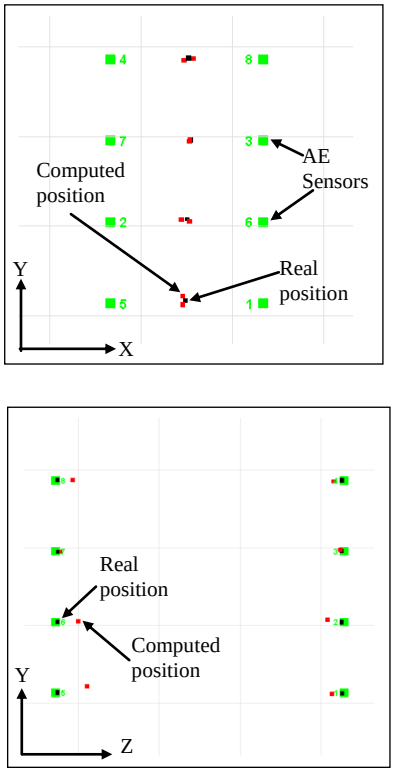

Figure 3: Estimation of error in AE source location.

This procedure allows estimating on one hand the speed of propagation and on other hand the attenuation of acoustic waves in the material [4]. The propagation velocity measured in our study is 3,800 m/s.

3 RESULTS

Figure 4 presents the average Force-Notch Mouth Opening Displacement (NMOD) curve of the beams. The variation between different beams is shown by gray zone.

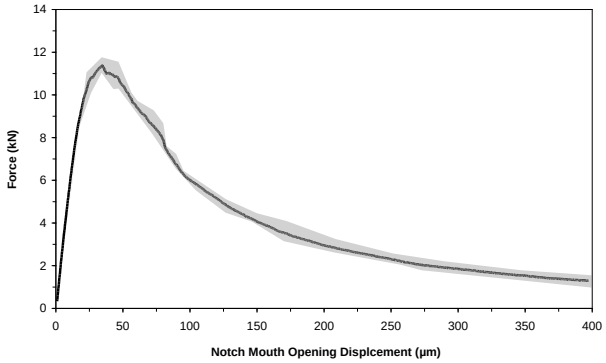

Figure 4: Average Force-Notch mouth opening displacement curve.

In the above curve, the relationship between the applied force and NMOD can be divided into four parts [2]. In the first part, the relationship is linear i.e. the material remains in the elastic range. The second part starts as soon as the curve deviates from linearity indicating the development of damage in the material. In this part, the load continues to increase further until the peak load value is reached.

After the peak load stage, NMOD continues to increase and the load starts to decrease. This is the third part of the curve, where a major load drop occurs. A shift in the Force-NMOD relationship is observed in the tail of the curve (at about 60% of peak load). This final part of the curve shows a considerable increase in the crack opening, while the load decreases gradually. The NMOD continues to increase until the specimen fails.

The above stages are the typical trends observed in the beams tested. These stages are no doubt related to the crack propagation in the material but this information is not available in the mechanical curve.

3.1 Analysis of crack openings using DIC

The process of DIC consists of analyzing a series of images of the specimen surface having a distributed grey level pattern. These patterns are monitored during the load application by a digital camera and stored in a computer in a digital format. Displacements fields can be measured by matching the first image (or the reference image, typically corresponding to the unloaded stage) and each subsequent image.

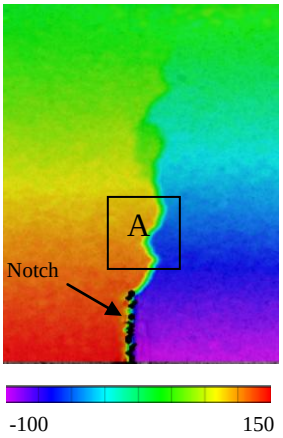

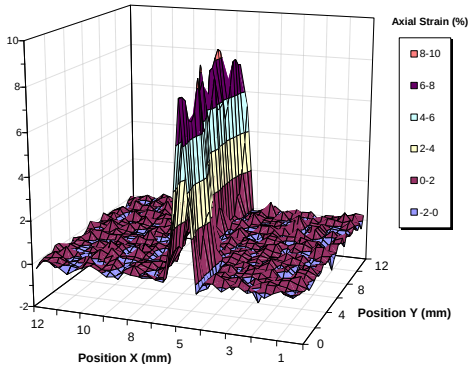

Figure 5: (a) Axial displacement (µm) (b) Axial displacement field in the area A.

The correlation algorithm determines the location of each sub-pixel in the imaging area. It provides the corresponding displacement vectors in the coordinate axis. The horizontal (axial) displacement can be easily calculated from the displacement vectors. Figure 5 presents the axial displacement field on the surface of the beam specimen at peak load. A sudden jump in the displacement values can be observed ahead of the notch and it represents a discontinuity (crack) in the material. Crack path can be determined easily from this figure.

Crack openings can be obtained from the displacement field [1]. It is the displacement jump across the two sides of the crack. In figure 6, crack openings profiles are drawn at different loading. The profiles are approximately the same on both sides of the specimen.

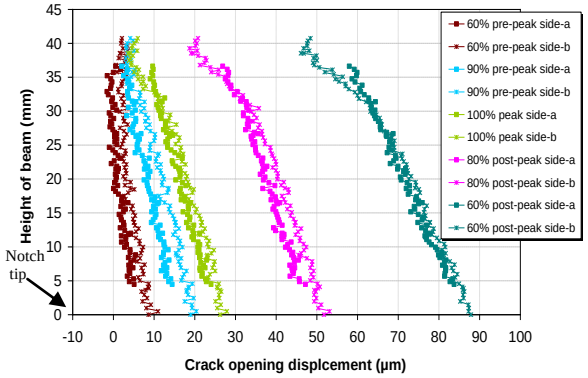

Figure 6: Crack opening profile on two faces of the beam.

In all the experiments the digital images are stored at a rate of 15 images per minute. The correlation of these images with respect to the reference image (unloaded specimen) provide the crack opening at different crack locations and thus crack opening rate can also be calculated at each interval of time. In Figure 7 the crack opening rate at three different crack locations is presented.

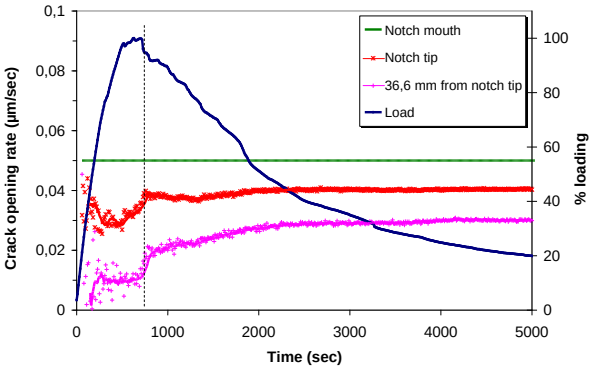

Figure 7: Crack opening rate at different locations in the beam

- At notch mouth, the opening rate is constant as it is controlled by the CMOD gauge.

- At notch tip (after a few unstable measurements at the beginning), the crack opening rate decreases while the load increases. In this part of the curve, the material behavior is in the elastic range and the decrease of crack opening rate may be due to the resistance of material to the opening of crack. The rate then starts to increase with further increase of the load. This increase of the crack opening rate represents the localization of microcracks. This continues until the specimen reaches its maximum load limit. After the peak load, the crack opening continues to increase at constant rate which indicates that the crack surfaces are now completely separated at the notch tip. It is also observed that the crack opening rate at the notch tip is always less than the crack opening rate at the notch mouth.
- At 36.6 mm from the notch tip, the crack opening rate increases suddenly just after the peak load. After this sudden increase, the crack opening rate increases smoothly and then it becomes constant. Again it is observed that the crack opening rate is always less than that at the notch tip and the notch mouth.

The crack can sometimes be interlocked by an aggregate. This aggregate interlock or aggregate shielding is observed in our experimental study (figures 8,9). An aggregate particle usually comes into the path and causes the crack to deflect. Sometimes aggregate particles also break due to a higher stress state in that location. In this case, aggregate interlock occurs just in front of the notch and causes an immediate drop of the crack opening.

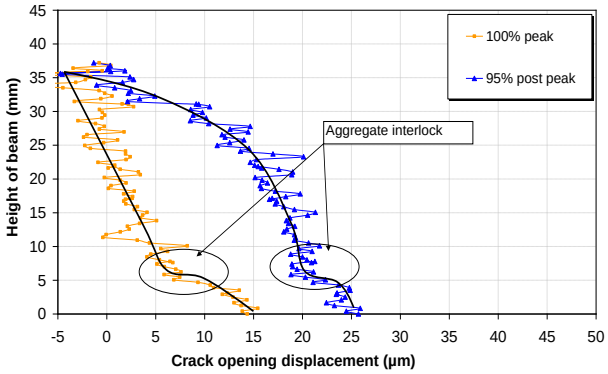

Figure 8: Crack opening profiles showing aggregate interlock.

It can also be seen that the crack extension is almost insignificant during the phase of aggregate interlock (Figure 8,9). Thus, more energy is consumed to break the crack interlock than to extend the crack [2]. However, the crack continues to extend as soon as the aggregate interlock is resolved. In this case, crack interlock is resolved by crack deflection. We can see in figure 9 that the crack path at the interlock location is not the same for 100% peak load and 80% post-peak load i.e. when the aggregate interlock is resolved. It is also observed that after the crack extends rapidly, it attains a "normal" crack length similar to other specimens where no aggregate interlock is observed.

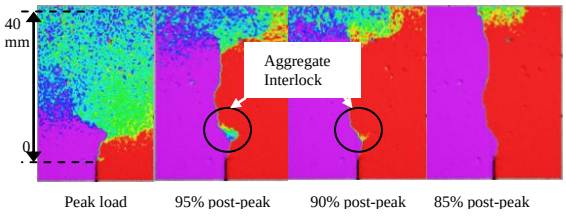

Figure 9: Crack propagation in a specimen showing aggregate interlock.

From the crack opening profiles, the crack length (measured from the notch tip) can be approximately located considering where the COD becomes equal to zero (i.e. crack closure). Actually, the crack tip is "blurred" by microcracking in the Fracture Process Zone (FPZ) and the COD gives the cumulative crack openings of all the microcracks in the FPZ. Therefore, the crack length measured in this way is the length of the macrocrack plus the

length of the FPZ where microcracks exist. This indicator can be very useful to study the durability of concrete structures, especially for cases where minor cracks can cause serious damage.

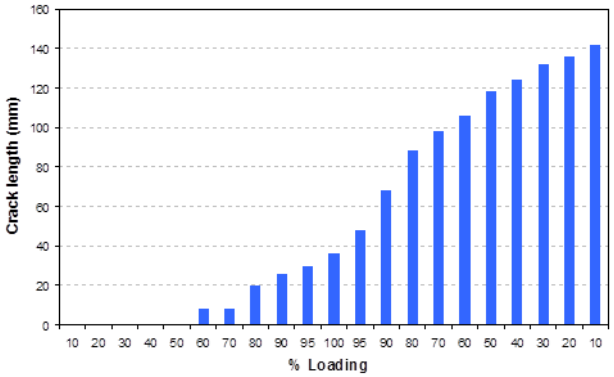

Figure 10: Evolution of crack length calculated from notch tip with load steps.

The crack length measured with DIC is plotted at different loading stages in figure 10. The crack appears at about 60% of the peak load in the pre-peak regime. This loading stage also corresponds to the sudden increase in the crack opening rate at the notch tip (figure 7) and the deviation of the mechanical behavior from linearity. The crack length increases smoothly until the peak load. A sudden increase in crack length is observed between the peak load and 80% of the peak load in the post-peak regime. The crack propagation becomes relatively slower in the final loading stages until the specimen fails completely.

3.2 Analysis of fracture process zone by AE

In this paper, we applied simultaneously DIC and AE techniques. In the first method only a small section of the sample is examined, which does not really represent the population of cracks and inaccessible areas are still unknown. Also DIC method is incapable to give information about the development and size of fracture process zone.

The AE technique is a passive method that identifies defects only when they develop under loading. An advantage of this technique is that it allows observation of the growth of damage zone (where fracture energy is released) in the tested material during the loading history, without moving the specimen.

Figure 11 shows a 3D localization of AE events in the three-point bending test. In this test the total number of events is equal to 2287.

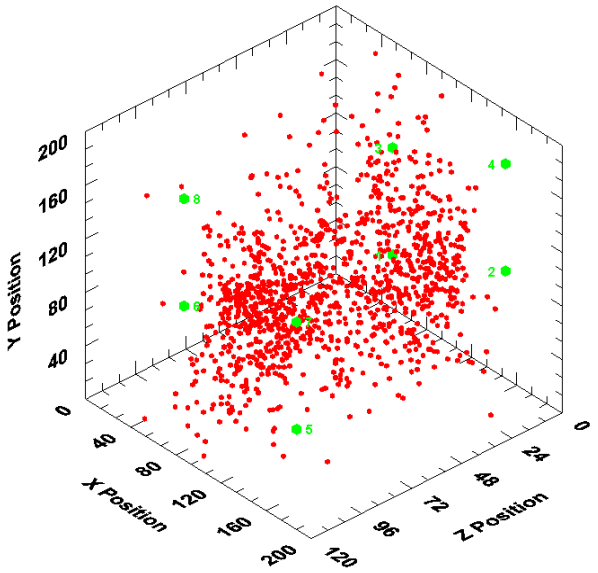

Figure 11: Localization of AE events in the beam.

One objective of the AE analysis is to compare the characteristics of the FPZ, and more particularly to know quantitatively the change in its width in the different phases of rupture.

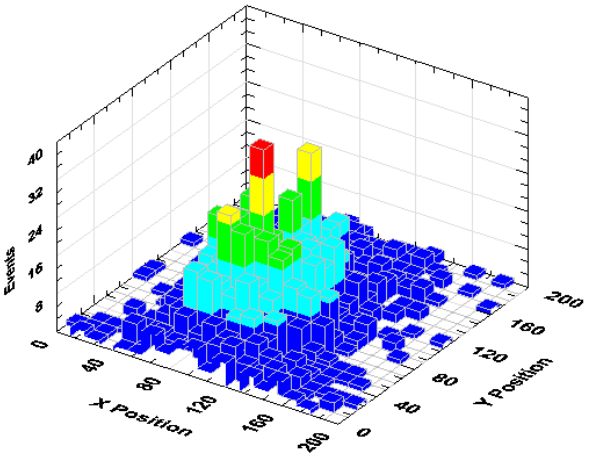

Figure 12: Distribution of AE events on the rectangular grid at final load step

The approach used here is similar to that developed by [5]. The beam surface is divided into a two dimensional (XY) grid of square

elements with uniform dimensions (1x1 cm^2). For each element the number of AE events is recorded. Figure 12 shows the total number of AE events located inside each grid element. Greater number of events is present above the notch which shows the localization of microcracking. Crack path can also be defined easily by knowing the total number of AE events as shown in figure 12.

In order to monitor the width of FPZ, cumulative number of AE events is recorded for each X location. This step is performed at different loading intervals. Figure 13 shows the cumulative number of events in the post-peak loading step. It can be seen that the number of AE events is more important in the zone above the notch and decreases gradually on both sides. To evaluate the width of FPZ (W_{FPZ}), we consider an arbitrary horizontal line located at 20% of N_{max} (N_{max} corresponds to the peak of the cumulative AE events). Thus W_{FPZ} can be identified as (i) the zone in which cumulative AE events at each X location is more than or equal to 20% of N_{max}. This zone corresponds to a zone of confidence in which the high number of events is representing the material damage or localization of microcracking (ii) the zone outside this zone (i), where cumulative AE events are lower than 20% of $N_{max,}$ corresponds to a lower level of damage [6].

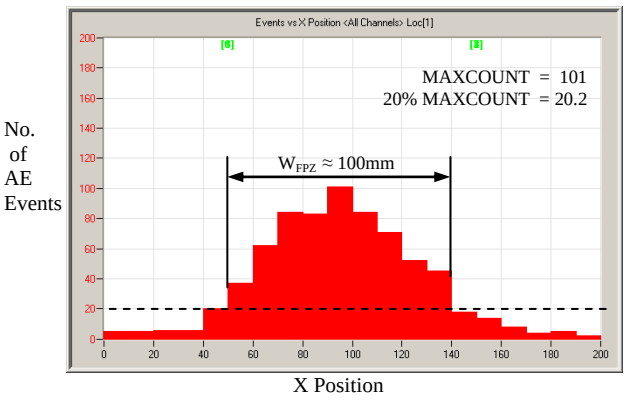

Figure 13: Cumulative AE counts at each X location and calculation of W_{FPZ}.

In our study the length of the FPZ (L_{FPZ}) is measured in the same way. L_{FPZ} should be the length of microcracking zone ahead of the stress free crack. However, alone AE analysis does not give information about the tip of the stress free crack. Figure 14 shows the cumulative number of events at each Y location in a post-peak loading step. It can be seen that ahead of the notch tip, the number of AE events increases, attains the maximum value (N_{max}) and then decreases. Therefore L_{FPZ} is taken as the length from notch tip to the intersection of the histogram with an arbitrary horizontal line located at 20% N_{max}.

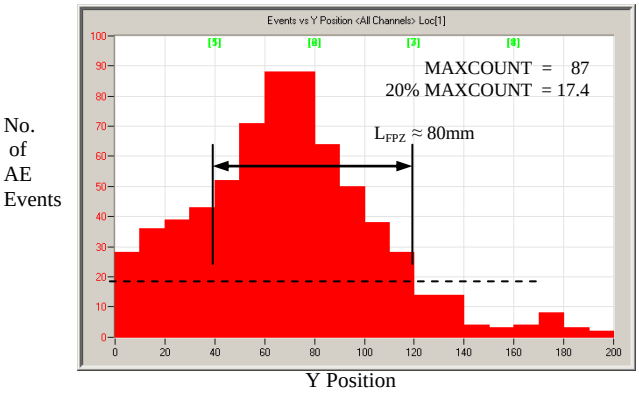

Figure 14: Cumulative AE counts at each Y location and calculation of L_{FPZ}.

In addition to the number of events, it is very important to investigate the AE signal parameters. The initiation and propagation of cracks in concrete are generally correlated to the study of AE signals of certain amplitude. Extensive studies have shown that the absolute acoustic energy is the most important parameter to characterize an event and not the amplitude [6,7]. In this study AE events are classified in terms of their level of energy. Therefore, seven energy levels are defined as shown in figure 15. It can be seen that the AE events of higher energy levels are located in a narrow zone and only the events having energy level greater than 70% of the total energy represents the core of fracture process zone [8]. So AE events having more than 1000 aJ of energy should be used to analyze the size of FPZ. Now applying this energy filter and previously described approach, W_{FPZ} and L_{FPZ} are again measured for different loading levels. Effect on L_{FPZ} is not very pronounced but a significant reduction in W_{FPZ} is observed. For the same loading level, W_{FPZ} reduced from

100 mm to 40 mm when using the energy filter.

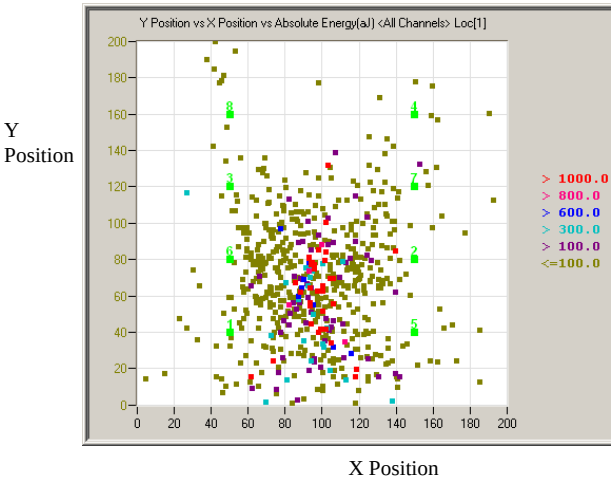

Figure 15: Acoustic Emission location map with energy discretization.

3.3 Combination of fracture data from DIC and AE

In this experimental study, Digital Image Correlation (DIC) is applied simultaneously with Acoustic Emission (AE) technique to study the fracture process in concrete beams. The advantage of combining the data obtained from the two techniques on the same experiment is that relation between microcracks and macrocrack can be build. Also the location of crack tip and the evolution of size of FPZ around the crack tip can be correctly estimated.

The progression of cracking in the beam at different loading conditions is presented in figure 16. Both the crack length growth measured using DIC and the increase of total number of AE events are the relative measure of damage accumulation in the beam. It can be observed that appearance of cracking using AE technique is near the peak load. On the other hand, appearance of crack is detected by DIC at 60% pre-peak loading. Similar experimental studies from other researchers also show the appearance of crack in the pre-peak loading regime. This also explains the nonlinear stress strain behavior in the pre-peak loading.

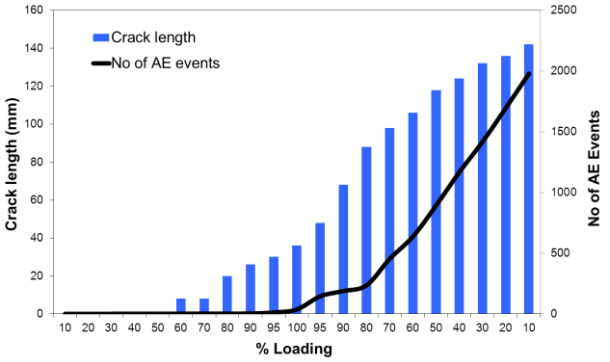

Figure 16: Evolution of crack length (measured using DIC) and cumulative number of AE events detected.

The crack length can also be detected from AE technique as shown in section 3.2. Figure 17 presents the crack length evolution as detected by DIC and AE techniques. It is observed that crack length measured from DIC is always larger than AE technique. It is very difficult to provide the relation between the two. As shown in section 3.1, DIC measures macrocrack length plus the length of FPZ where microcracks are open.

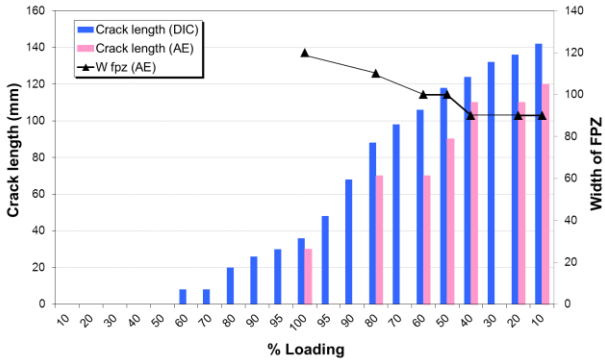

Figure 17: Evolution of crack length and W_{fpz} using DIC and AE.

The evolution of width of fracture process zone W_{fpz} using AE technique is also shown in figure 17. It can be observed that W_{fpz} is maximum at peak load. At this loading step W_{fpz} is estimated to be 120 mm which is ten times the maximum aggregate size. After the peak load, W_{fpz} decreases and then remains constant after 50% of post-peak load.

12 CONCLUSIONS

In this paper an experimental study is presented in order to study the fracture growth

during three point bending tests in concrete beams. Two techniques DIC and AE were employed. The conclusions are

- It is found that DIC and AE can be used simultaneously with no experimental issues. Real time experimental data can be easily collected.
- DIC is an effective method to measure discontinuities such as crack length and crack openings. Fracture process zone width can be easily monitored with AE technique.
- Crack length measured with DIC is more important than that from AE. The reason may be that measurement of crack length from DIC is based on crack openings. It includes the macrocrack length but also part of FPZ where microcracks are open.
- It is observed with DIC and AE that crack advances more rapidly after the peak load. During this early post-peak phase, decrease of W_{fpz} is observed. After 50% post-peak loading, W_{fpz} becomes uniform.
- W_{fpz} is more important at the beginning because the cracking is more distributed and therefore the measured W_{fpz} is higher at the peak load. When the macrocrack starts to propagate (after peak load) AE events are usually located in the middle. Thus, the measured W_{fpz} starts to decease.

REFERENCES

[1] Alam S.Y., Loukili A. and Grondin F., 2012. Monitoring crack openings in concrete beams with different sizes using digital image correlation technique. *Eur J Environ Civil Eng*. **16(7):818-813**.

[2] Saliba J., Loukili A., Grondin F. and Regoin J.P., 2012. Influence of basic creep on cracking of concrete shown by the Acoustic Emission technique. *Mater Struct*. **45:1389-1401**.

[3] Granger S., Loukili A., Pijaudier-Cabot G. and Chanvillard G., 2007. Experimental characterization of the self-healing of cracks in an ultra high performance cementitious material: mechanical tests and acoustic emission analysis. *Cem Concr Res*. **37:519-527**.

[4] RILEM TC212-ACD recommendation, 2010. Acoustic emission and related NDE techniques for crack detection and damage evaluation in concrete. *Mater Struct* **43:1177-1181**.

[5] Haidar K., Pijaudier-Cabot G., Dubé J.F. and Loukili A., 2005. Correlation between the internal length, the fracture process zone and size effect in model materials. *Mater Struct*. **38:201–210**.

[6] Hadjab H.S., Thimus J.F. and Chabaat M., 2007. The use of acoustic emission to investigate fracture process zone in notched concrete beams. *Curr Sci*. **93(5):648-653**.

[7] Muralidhara S., Raghu Prasad B.K., Eskandari H. and Karihaloo B., 2010. Fracture process zone size and true fracture energy of concrete using acoustic emission. *Constr Build Mater*. **24:479-486**.

[8] Otsuka K. and Date H., 2000. Fracture process zone in concrete tension specimen. *Eng Fract Mech.* **65(2-3):111-131**.